

Extreme Environmental Thermal Shock Induced Dislocation-Rich Pt Nanoparticles Boosting Hydrogen Evolution Reaction

Siliang Liu, Yi Shen, Yang Zhang, Baihua Cui, Shibo Xi, Jinfeng Zhang, Lianying Xu, Shuze Zhu, Yanan Chen,* Yida Deng, and Wenbin Hu


Crystal structure engineering of nanomaterials is crucial for the design of electrocatalysts. Inducing dislocations is an efficient approach to generate strain effects in nanomaterials to optimize the crystal and electronic structures and improve the catalytic properties. However, it is almost impossible to produce and retain dislocations in commercial mainstream catalysts, such as single metal platinum (Pt) catalysts. In this work, a non-equilibrium high-temperature (>1400 K) thermal-shock method is reported to induce rich dislocations in Pt nanocrystals (Dr-Pt). The method is performed in an extreme environment (≈ 77 K) created by liquid nitrogen. The dislocations induced within milliseconds by thermal and structural stress during the crystallization process are kinetically frozen at an ultrafast cooling rate. The high-energy surface structures with dislocation-induced strain effects can prevent surface restructuring during catalysis. The findings indicate that a novel extreme environmental high-temperature thermal-shock method can successfully introduce rich dislocations in Pt nanoparticles and significantly boost its hydrogen evolution reaction performance.

1. Introduction

Hydrogen energy is an important alternative to fossil fuels that can help to realize the goal of carbon neutrality.^[1] As a promising hydrogen production technique, the electrocatalytic decomposition of water, which comprises the hydrogen evolution reaction (HER) and oxygen evolution reaction (OER), has received increasing attention.^[2] It has the advantages of facile reactant accessibility, large-scale production feasibility, and high product purity.^[3] According to the Sabatier principle, platinum (Pt)-based metals with a d_9 electronic structure simultaneously possess moderate HER intermediate absorption energy and satisfy the HER performance in acidic media.^[4] This catalyst is believed to be the most promising for electrocatalytic water decomposition. The key challenge of Pt-based catalysts lies in their

S. Liu, J. Zhang, Y. Chen, Y. Deng, W. Hu
School of Materials Science and Engineering
Key Laboratory of Advanced Ceramics and Machining Technology of
Ministry of Education
Tianjin Key Laboratory of Composite and Functional Materials
Tianjin University
Tianjin 300072, China
E-mail: yananchen@tju.edu.cn
Y. Shen, S. Zhu
Department of Engineering Mechanics
Institute of Applied Mechanics
School of Aeronautics and Astronautics
Zhejiang University
Zhejiang 310027, China
Y. Zhang, L. Xu
School of Materials Science and Engineering
Key Laboratory of Advanced Joining Technology
Tianjin University
Tianjin 300072, China

B. Cui
Department of Chemistry
National University of Singapore
Singapore 117543, Singapore
B. Cui, W. Hu
Institute of Chemical and Engineering Sciences
A*STAR, 1 Pesek Road, Jurong Island, Singapore 627833, Singapore
S. Xi
School of Materials Science and Engineering
Hainan University
Haikou 570228, China
Y. Deng
Joint School of National University of Singapore and Tianjin University
International Campus of Tianjin University
Fuzhou 350207, China

 The ORCID identification number(s) for the author(s) of this article can be found under <https://doi.org/10.1002/adma.202106973>.

DOI: 10.1002/adma.202106973

slower HER kinetics in alkaline media compared to those in acidic media. This is due to the sluggish step of splitting water into hydrogen intermediates (H_{ad}) and desorption of H_{ad} . Therefore, exploring the maximum potential of Pt in the generation and desorption of H_{ad} to boost HER electrocatalysis in alkaline media is of great significance.

Regulating the electronic structure on the catalyst surface is an effective strategy to improve the reaction potency of noble metal-based electrocatalytic water splitting, which can be typically tuned by defect engineering.^[4b,5] Defects induce strain fields, which regulate the electronic structure of the adsorption site to improve the interaction between the adsorbed intermediates and the adsorption site.^[4b,5c,d,6] However, defects are often accompanied by changes in the coordination number (CN) on the surface structures of metal catalysts, which affects the catalytic performance of the active sites.^[4b,7] Defects that are effective in improving the electrocatalytic reaction efficiency can be categorized as point defects (vacancies, etc.), line defects (dislocations, etc.), and plane defects (grain boundaries, etc.). For example, Kanna et al.^[8] proposed that dislocations and grain boundaries can promote the CO_2 electroreduction reaction because of the increase in undercoordinated sites induced by defects. As a typical type of bulk defect, dislocations can induce a strain effect to optimize the electronic structure of the catalysts effectively and is more stable during the catalytic process compared with surface defects.^[5d,8,9]

High-temperature thermal shock (HTS) is a non-equilibrium extreme method for introducing dislocations into electrocatalysts, such as IrNi alloy nanoparticles.^[9b] However, the current reaction and kinetic condition of HTS are still insufficient to form rich dislocations in Pt single metal electrocatalysts, owing to its small size and high crystallization process. To further secure dislocations in Pt, we used liquid nitrogen as the cooling medium to create a more extreme kinetic reaction condition in

HTS, which can both promote and retain the dislocations in Pt single metal catalysts.

In this study, a facile non-equilibrium HTS method is proposed to generate dislocation-rich single Pt nanoparticles (Dr-Pt) in an extreme environment by introducing a liquid nitrogen cooling medium. Compared with Dr-Pt, the Pt nanoparticles prepared in an argon (Ar) atmosphere (Dp-Pt), that is, a normal temperature and pressure environment, displayed poor dislocations. The strain effect induced by dislocations mediated the electronic structure and optimized the catalytic activity of Dr-Pt, including reduced overpotential and increased stability. Compared with Dp-Pt (with an overpotential of ≈ 45 mV at 10 mA cm^{-2}), Dr-Pt exhibited a lower overpotential (≈ 25 mV at 10 mA cm^{-2}) in 1 M KOH solution. Dr-Pt also showed high electrocatalytic stability under continuous testing for 20 h and structural stability (Figure S8, Supporting Information) with well-retained dislocations after the long-term reaction. This work highlights the potential of environmental thermal shock in inducing dislocations within Pt nanoparticles to achieve more competent electrocatalysts, which could facilitate the design of different defect-rich nanomaterials.

2. Results and Discussion

The schematic diagram in **Figure 1** depicts the HTS process for the preparation of Dr-Pt in a liquid nitrogen medium and the mechanism of the formation of dislocations. After thermal shock, H_2PtCl_6 instantly decomposes into Pt and Cl atoms (Figure 1a). As chloroplatinic acid lacks a thermodynamically stable molecular structure, H_2PtCl_6 is replaced by $PtCl_4$. The Cl atoms can form chlorine gas and escape. Pt atoms can aggregate on carbon nanotubes (CNTs) at an ultrafast speed

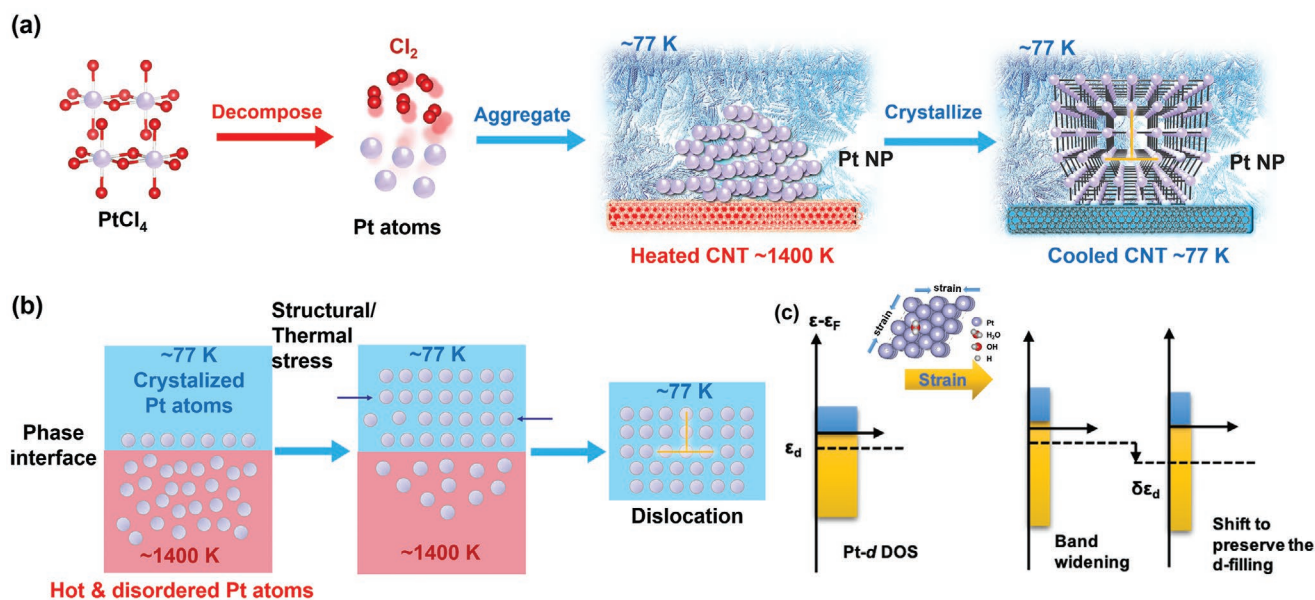


Figure 1. Schematic diagram of the preparation of dislocation-rich Pt nanoparticles by environmental HTS. a) H_2PtCl_6 was decomposed into Pt atoms and chlorine gas. The Pt atoms quickly condensed and crystallized to Dr-Pt on the CNT. b) The structural and thermal stresses act together on the Pt nanoparticle, triggering the formation of dislocations. The extreme fast cooling rate kinetically freezes the dislocations. c) Changes in the Pt d-band structure upon compressive strain.

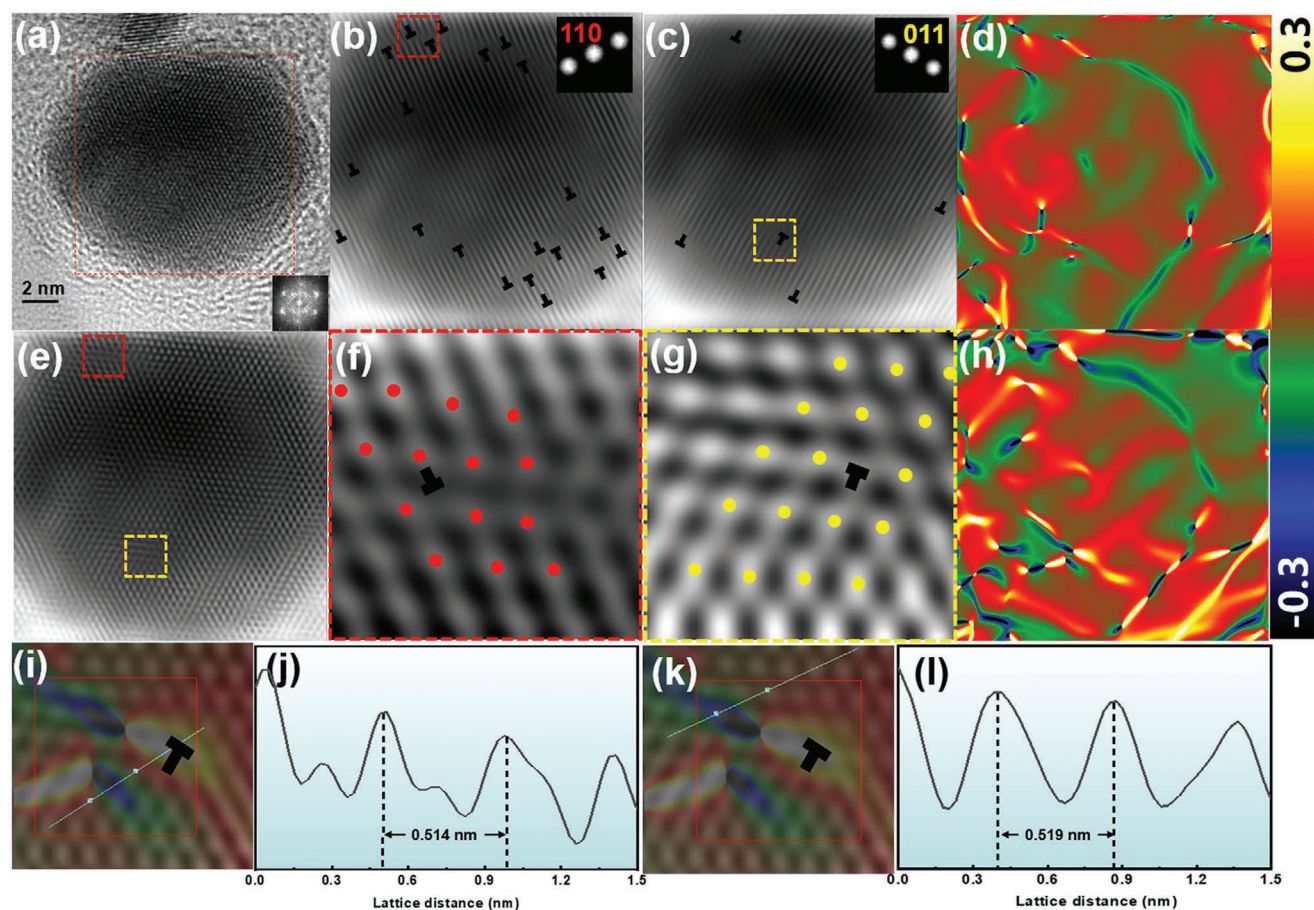


Figure 2. Structural characterization of Dr-Pt nanoparticles. a) HRTEM image of the Dr-Pt nanoparticle. b,c) IFFT patterns of the (110) and (011) plane of the Pt nanoparticle, corresponding to the square area in (a), exhibiting numerous dislocations marked with “T”, respectively. d,h) Strain distributions of ϵ_{xx} and ϵ_{yy} , which is related to the (110) and (011) planes. e) Filtered IFFT pattern of the Pt nanoparticle in (a) containing all the plane information. f,g) Enlarged areas corresponding to the areas marked in (e), containing surface dislocations where the atom columns are marked with colored circles. i–l) The interplanar spacing analysis of surface dislocations in (f,g). (The tensile strain is represented by red to bright yellow, while compressive strain is depicted by green to dark blue.)

as the heat holding time is only ≈ 20 ms. During the crystallization process, the structural stress can be induced at the joint between the uncrystallized Pt atoms and the crystallized Pt atoms. The thermal stress caused by the temperature gradient across the nanoparticles also has significant effects on the atomic structure. As shown in Figure 1b, these two stresses act together on the Pt nanoparticles, induce plastic deformation in the local area, and trigger the formation of dislocations. The extremely fast cooling rate also causes the generated dislocations to be kinetically frozen in the nanoparticles. The strain induced by the rich dislocations downshifts the d-band center of Pt (Figure 1c). As the d-band center downshifts, antibonding d states move toward the Fermi level accompanied by increased occupation, leading to weakened adsorption energy between the metal and reaction intermediates.

A representative high-resolution transmission electron microscopy (HRTEM) image of Dr-Pt is shown in Figure 2a. The particle size of Dr-Pt is ≈ 15 nm, and the inset image shows the corresponding fast Fourier transform (FFT) pattern. The places marked with “T” are dislocations. Figure 2b,c shows the inverse FFT (IFFT) images of Figure 2a, which are related to the (110)

and (011) planes, respectively. Figure 2d–h shows the Geometric Phase Analysis (GPA) images of the (110) and (011) planes, respectively. It can be seen that dislocations introduce significant strain effects on the particles. In addition to observing the dislocations inside the particle, we also observed the dislocations on the surface of the particle, as shown in Figure 2e–g, which correspond to the red and yellow frames marked areas in Figure 2b,c. The atomic columns of the dislocations are marked with red and yellow spots. Note that the extra half atomic plane in the dislocation on the surface causes distortion of the surrounding lattice of the Pt nanoparticle (Figure 2f,g). Figures 2i–l show the strain distribution in the area where the surface dislocations of Pt nanoparticles are located and the interplanar spacing of the (110) plane of the compressed area, respectively. The interplanar spacing of the (110) plane of the Pt nanoparticle is 0.26–0.265 nm, which is compressed by ≈ 5 –5.8% than the theoretical interplanar spacing $d_{(111)} = 0.276$ nm. In addition, we analyzed the dislocations of Dp-Pt nanoparticles prepared in an Ar atmosphere and Pt nanoparticles in a 20 wt.% commercial Pt/C catalyst. As shown in Figure S2, Supporting Information, the Dp-Pt nanoparticles contained only a few dislocations,

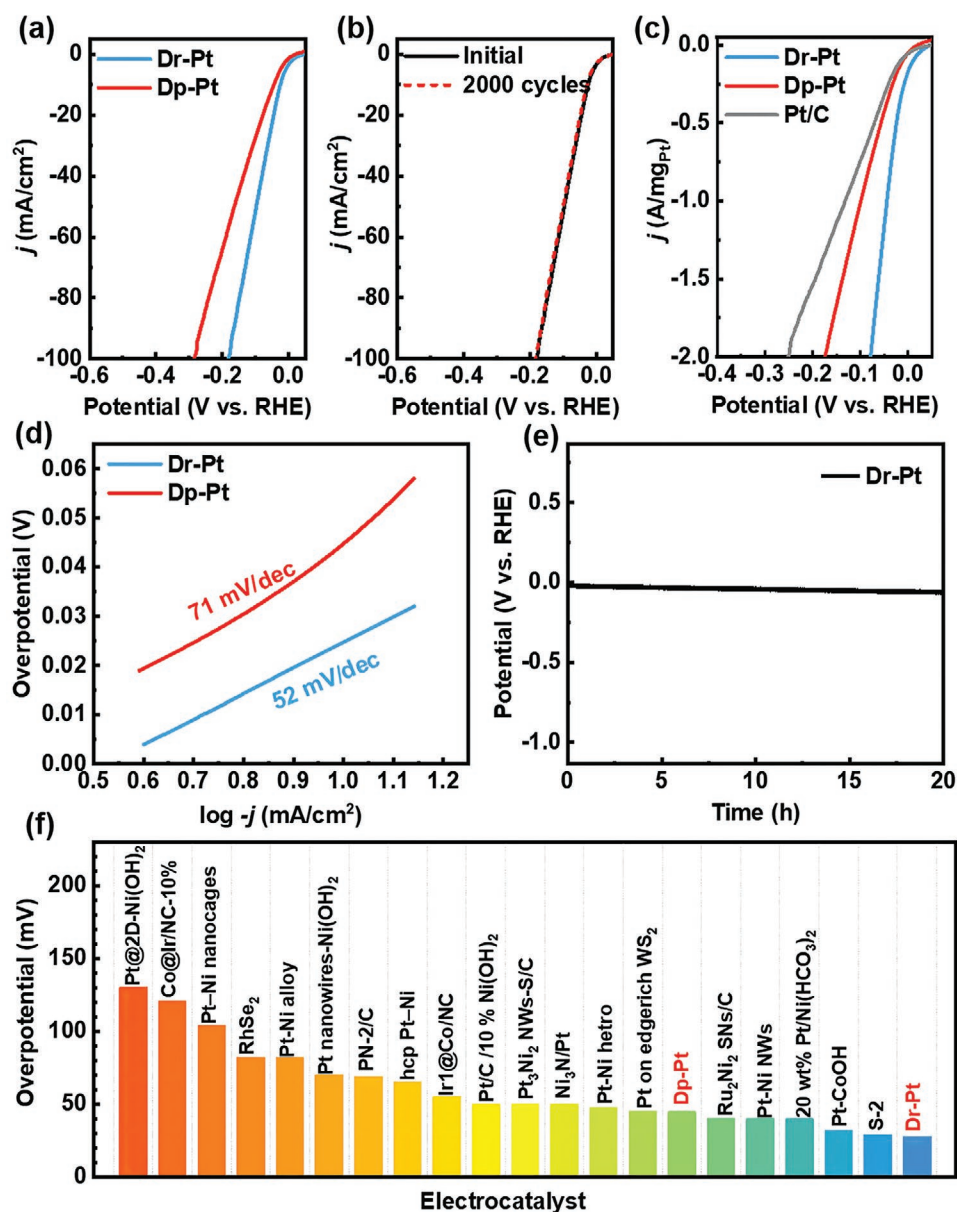


Figure 3. HER activity and durability evaluation of Dr-Pt. a) LSVs of Dr-Pt and Dp-Pt measured at 5 mV s⁻¹. b) Polarization curves of initial and after 2000 cycles. c) Mass activity comparison of catalysts. d) The Tafel plots of catalysts. e) Current–time Chronopotentiometric curve of Dr-Pt at 10 mA cm⁻². f) Comparison of the overpotentials at 10 mA cm⁻² between Dr-Pt and other state-of-the-art electrocatalysts.

while no dislocation was observed in the Pt nanoparticles of the commercial Pt/C catalyst. Therefore, the extreme environment induced by liquid nitrogen can quickly “freeze” the dislocations in the Dr-Pt nanoparticles.

The HER activity of the above Pt catalysts was tested in the N₂-saturated 1 M KOH electrolyte using a graphite rod as the counter electrode without insulation resistance compensation. As shown in Figure 3a, compared to Dp-Pt, the HER activity of Dr-Pt was obviously improved. Specifically, Dr-Pt exhibited excellent HER activity with a low overpotential of 26 mV at a current density of 10 mA cm⁻². As shown in Figure 3d, the Tafel slope of Dr-Pt of 52 mV dec⁻¹ is much lower than that of Dp-Pt (45 mV, 71 mV dec⁻¹) and other state-of-the-art electrocatalysts

(Figure 3f). As presented in Figure 3c, the mass activities at the overpotential of 50 mV of Dr-Pt, Dp-Pt, and commercial 20 wt.% Pt/C are calculated as 1.16 A mg⁻¹_{Pt}, 0.42 A mg⁻¹_{Pt} and 0.32 A mg⁻¹_{Pt}. The cyclic stability of Dr-Pt was demonstrated by comparing the initial linear sweep voltammetry (LSV) plots and after 2000 cyclic voltammetry sweeps, from 0.05 to -0.3 V versus reversible hydrogen electrode (RHE) at 50 mV s⁻¹, in a 1 M KOH solution to further evaluate the long-term durability, as shown in Figure 3b. The Dr-Pt catalyst exhibited negligible decay after 2000 cycles. Furthermore, chronopotentiometric measurement was performed at a current density of 10 mA cm⁻² (Figure 3e), indicating that Dr-Pt exhibits a negligible reduction in catalytic stability and activity after 20 h.

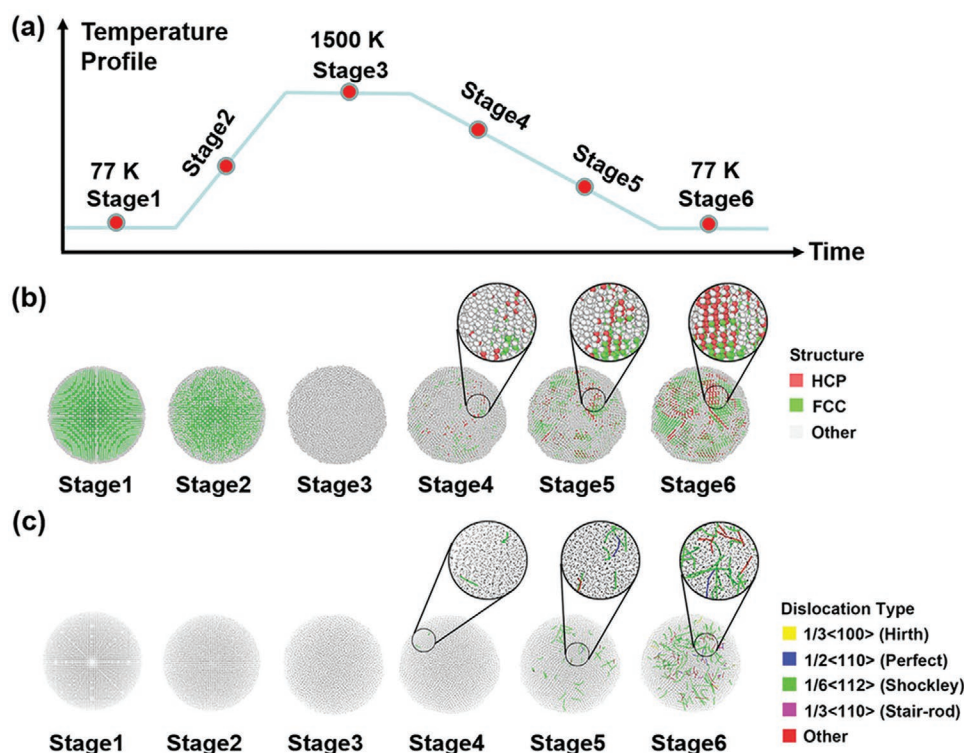


Figure 4. Molecular dynamics simulation analysis of 10 nm Pt particles during rapid heating and cooling, with a maximum temperature of 1500 K. a) The temperature profile of the simulation. b) The crystal structure of a nanoparticle at each stage. c) The evolution of dislocations at different stages, where the dislocations are colored according to their categories.

We further performed molecular dynamics (MD) simulations to demonstrate that the ultrafast heating and cooling process could induce abundant dislocations in a Pt nanoparticle. By analyzing the temperature state, the crystal structure change of the nanoparticle, and the dislocation structure change in the simulation process, the dynamic process of dislocation formation was elucidated. The Pt nanoparticles were first equilibrated at 77 K and then heated to 1500 K, as shown in Figure 4a. The temperature difference in the Pt nanoparticles induces thermal stress, with the corresponding formation of rich dislocations. Figure 4b shows the evolution of the atomic structure during HTS. The rapid cooling process completely changes the atomic environment inside the Pt particles, making them different from ordinary Pt particles. Figure 4c shows the evolution of the dislocations at six different stages. Dislocations do not emerge at the heating and insulation stages, but begin to emerge at the cooling stage. This may be due to the non-uniformity of the temperature of each local part of the Pt particle during cooling, which results in thermal stress. Almost all of the initial dislocations were of the Shockley type at stage 4. As the temperature of the Pt particle continues to decrease, the dislocations begin to grow, and the number and length of the dislocations increase rapidly. Through stage 5, new types of dislocations gradually appeared. At stage 6, abundant dislocations form and the Shockley type still predominates.

To further investigate the nature of the high activity of Dr-Pt, systematic density functional theory (DFT) calculations using the Vienna Ab initio Simulation Package with

the generalized gradient approximation approach were performed.^[10] Based on the experimental results, we constructed Pt-(111) models with strain effects of -5%, 0%, 5%, and 10%, represented as Pt-0.95, 1.00, 1.05, 1.10, respectively, as shown in Figure 5. HER performs Volmer–Heyrovsky/Tafel steps in alkaline condition (Volmer: $* + \text{H}_2\text{O} + \text{e}^- \rightleftharpoons \text{H}^* + \text{OH}^-$; Tafel: $2\text{H}^* \rightleftharpoons \text{H}_2$; Heyrovsky: $\text{H}^* + \text{H}_2\text{O} + \text{e}^- \rightleftharpoons \text{H}_2 + \text{OH}^-$, where $*$ represents the active position).^[11] The hydrogen adsorption free-energy (ΔG_{H^*}) is a suitable descriptor to evaluate the HER activity.^[12] $|\Delta G_{\text{H}^*}|$ is expected to be as small as possible to achieve the best HER activity. The Volmer step consists of the adsorption and dissociation of H_2O , and the Tafel/Heyrovsky step includes the desorption of H^* . According to the free-energy landscape of the HER process of Pt models (Figure 5a), the energy barriers of Pt-0.95, Pt-1.00, 1.05, and 1.10 are the dissociation of H_2O and desorption of H^* , respectively. Pt-0.95 exhibited the lowest $|\Delta G_{\text{H}^*}|$ and limiting potential, suggesting the best HER activity, as shown in Figure 5b. To understand the HER mechanism and explain why compressive strain can promote H^* desorption, Bader charge analysis with charge density differences of Pt models having different strain effects were performed. The color bar on the right in Figure 5c shows the electron cloud density of the model in e/bohr^3 . The H^* on the surface of model Pt-0.95 showed the least overlap of the electron cloud, indicating that the compressive strain weakens the H adsorption and accelerates the Tafel step. To further investigate the electron mutual effect of Pt atoms and adsorbates, the projected density of state (PDOS)

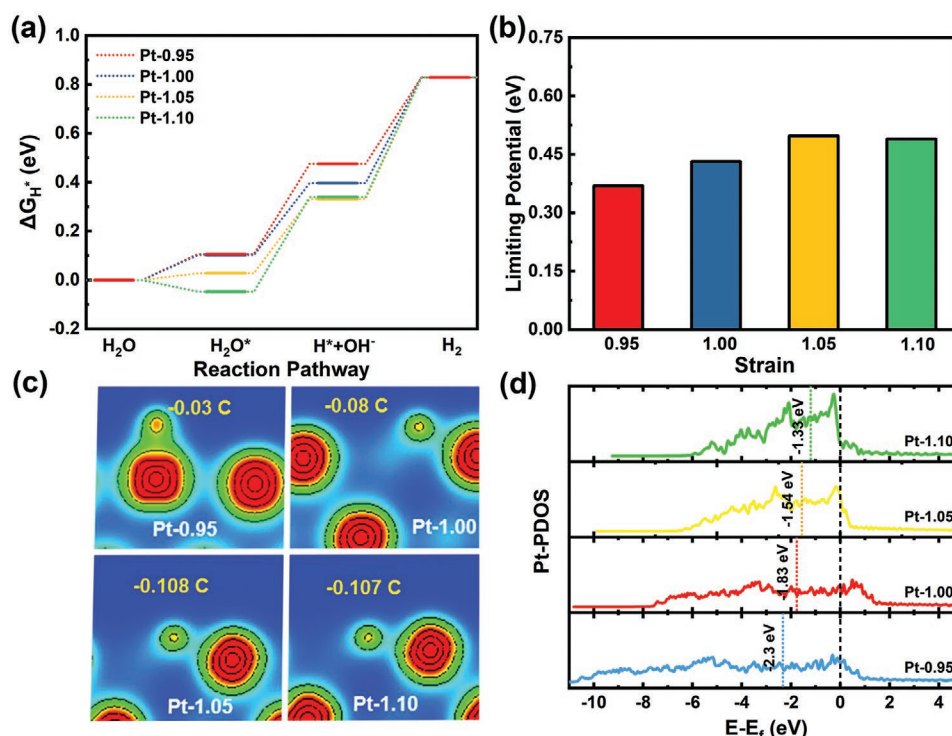


Figure 5. Theoretical calculation results of the strain effect on the electronic structures and HER activity of Dr-Pt. a) The free-energy landscape of HER process of Pt models under different strains. b) The limiting potentials of Pt models. c) Bader charge analysis of Pt. The color bar on the right shows the electron cloud density of the model in $e \text{ bohr}^{-3}$. d) PDOS profiles of surface Pt atoms under strain effects.

of the d-orbital electron on the surface of the Pt atom was analyzed (Figure 5d). Accordingly, the d-band center,^[13] which is applied to describe the binding strengths of the active sites and adsorbates, is calculated as being away from the Fermi level owing to the compressed structures, and the introduction of compressing strains downshifted the d-band center of Pt to the Fermi level, which is attributed to the strengthened Pt–Pt bond and impaired bonding strengths between Pt and hydrogen-containing adsorptions.

3. Conclusion

Using a non-equilibrium extreme environmental HTS method, we successfully prepared Dr-Pt. During the crystallization process, severe thermal stress and corresponding structural stress successfully induced rich dislocations in Dr-Pt. Dr-Pt, with a desirable strain effect induced by abundant dislocations, promotes water splitting efficiency and HER performance. MD simulations demonstrated dislocation formation due to fast heating and cooling, suggesting a temperature-guided thermal stress effect. DFT results further illustrated that the strain effect induced by dislocations can optimize the adsorption energy of H_{ad} by modulating the electronic structure of the Pt atoms. The findings prove that environmental HTS can facilitate the preparation of dislocation-rich single metal nanoparticles to enhance the HER performance and provide new guidance for the rational structural design of catalysts with abundant defects for hydrogen generation.

4. Experimental Section

Preparation of Materials: The chemical vapor deposition (CVD) process was used to synthesize CNTs.^[14] The CNTs was then dipped into the 0.03 M H_2PtCl_6 aqueous solution overnight, and dried in a vacuum freeze-dryer. Then, the salt-loaded CNTs was linked to a direct-current source and heated in liquid nitrogen. The current pulse across the salt-loaded CNTs was $\approx 3.1 \text{ A}$ for $\approx 0.02 \text{ s}$. For comparison purposes, Dp-Pt was prepared using the same heating parameter but in a normal temperature and pressure environment in an Ar-filled glovebox. The 20 wt% Pt/C catalyst (1 mg) was dispersed in a mixture solution which consists of 30 μL 5% nafion and 970 μL ethanol, and sonicated for 40 min, which was loaded on the glassy carbon electrode.

Characterizations: HRTEM was carried out on a JEOL JEM-ARM200F transmission electron microscope. The scanning electron microscopy (SEM) was performed using a JEOL JSM-7800F microscope. An infrared imaging device (ImageIR8355BBhp) was applied to obtain a series of infrared temperature images. GPA was conducted using the Digital Micrograph software. The extended X-ray absorption fine structure (EXAFS) measurements of Pt L3-edge were performed at the XAFCA beamline at the Singapore Synchrotron Light Source. A Si(111) double crystal monochromator was applied to monochromatize the incident X-ray beam. All samples were mixed with boron nitride powder, pressed into pellets. All the transmission-mode EXAFS spectra were measured by using ionization chambers at room temperature. Pt foil was used for X-ray energy calibration.

Electrochemical Characterization: The HER tests were conducted in an N_2 -saturated 1 M KOH solution at room temperature on a CHI 660E electrochemical workstation. The electrocatalysts-loaded CNTs/glassy carbon electrode, a saturated calomel electrode, and a graphite rod were used as the working, reference, and counter electrodes, respectively.

Cyclic voltammograms (CVs) were collected in the potential range of 0.168 to -0.532 V versus reversible hydrogen electrode (RHE) at 100, 50 and 20 mV s^{-1} until the active substances are activated. The LSV was

carried out in the same potential range of CVs without *iR* compensation. The cyclic durability test of Dr-Pt was conducted by potential sweeps in the potential range of 0.168 V to −0.232 V versus RHE at 50 mV s^{−1} in 1 M KOH solution.

Calculation Methods: The self-consistent field (SCF) tolerance was 1×10^{-8} eV with $6 \times 6 \times 1$ Monkhorst–Pack mesh *k*-points. The cutoff energy of 400 eV of plane-wave basis sets was assigned. The convergence criterion for atomic relaxation was 0.01 eV Å^{−1}. The eight-layer Pt (111) surface unit cell repeated in 3×3 was fully relaxed. A 15 Å vacuum width along the Z-axis between the slabs was applied to eliminate artificial interactions. The ΔG_{H^*} was computed by

$$\Delta G_{H^*} = E(\text{surf} + H) - E(\text{surf}) - \frac{1}{2}E(H_2) + \Delta E_{ZPE} - T\Delta S \quad (1)$$

where ΔS and ΔE_{ZPE} are the deviations of the zero-point entropy and energy between the H* and H₂. We used vaspkit to thermodynamically modify the energy of adsorbed states and gas molecules.^[15]

The free energy of H⁺ (10^{−14} M) + 1 e[−] can be calculated by applying a pH correction energy:^[16] $\Delta G(\text{pH}) = kT\ln[H^+] = -pH \cdot kT\ln 10$, where pH = 14.

Supporting Information

Supporting Information is available from the Wiley Online Library or from the author.

Acknowledgements

The authors acknowledge the financial support from the National Natural Science Foundation of China (52171219, 91963113, 12002304, U1601216, 51701139). The authors acknowledge the help from Dr. Anyuan Cao, Dr. Shi Hu, Dr. Qiang Li, Dr. Weidi Liu and Mr. Yizeng Wu.

Conflict of Interest

The authors declare no conflict of interest.

Author Contributions

S. L. and Y. C. conceived the idea and designed the experiment. Y. S. and S. Z. contributed the MD simulation. S. L., Z. Y., B. C., and J. Z. carried out the synthesis, characterization and electrochemical experiments. All authors participated in the data analysis and contributed to the manuscript writing.

Data Availability Statement

The data that support the findings of this study are available from the corresponding author upon reasonable request.

Keywords

dislocations, environmental thermal shock, hydrogen evolution reaction (HER), single metal nanoparticles, strain

Received: September 2, 2021

Revised: October 7, 2021

Published online: November 8, 2021

- [1] a) J. A. Turner, *Science* **2004**, 305, 972; b) Y. Shi, B. Zhang, *Chem. Soc. Rev.* **2016**, 45, 1529.
- [2] a) Y. Zhai, X. Ren, J. Yan, S. Liu, *Small Struct.* **2021**, 2, 2000096; b) L. Zhang, H. Zhao, S. Xu, Q. Liu, T. Li, Y. Luo, S. Gao, X. Shi, A. M. Asiri, X. Sun, *Small Struct.* **2021**, 2, 2000048; c) T. Ouyang, Y.-Q. Ye, C.-Y. Wu, K. Xiao, Z.-Q. Liu, *Angew. Chem., Int. Ed.* **2019**, 58, 4923; d) J.-X. Wei, M.-Z. Cao, K. Xiao, X.-P. Guo, S.-Y. Ye, Z.-Q. Liu, *Small Struct.* **2021**, 2100047.
- [3] a) Q. Lu, Y. Yu, Q. Ma, B. Chen, H. Zhang, *Adv. Mater.* **2016**, 28, 1917; b) Y. Zhu, Q. Lin, Y. Zhong, H. A. Tahini, Z. Shao, H. Wang, *Energy Environ. Sci.* **2020**, 13, 3361; c) P. Wang, X. Zhang, J. Zhang, S. Wan, S. Guo, G. Lu, J. Yao, X. Huang, *Nat. Commun.* **2017**, 8, 14580.
- [4] a) P. Sabatier, *Ber. Dtsch. Chem. Ges.* **1911**, 44, 1984; b) Z. Li, J.-Y. Fu, Y. Feng, C.-K. Dong, H. Liu, X.-W. Du, *Nat. Catal.* **2019**, 2, 1107; c) S. Bai, C. Wang, M. Deng, M. Gong, Y. Bai, J. Jiang, Y. Xiong, *Angew. Chem., Int. Ed.* **2014**, 53, 12120; d) J. K. Nørskov, C. H. Christensen, *Science* **2006**, 312, 1322.
- [5] a) X. Tian, X. Zhao, Y. Su, L. Wang, H. Wang, D. Dang, B. Chi, H. Liu, E. J. M. Hensen, X. W. Lou, B. Y. Xia, *Science* **2019**, 366, 850; b) L. Wang, Z. Zeng, W. Gao, T. Maxson, D. Raciti, M. Giroux, X. Pan, C. Wang, J. Greeley, *Science* **2019**, 363, 870; c) R. Chattot, O. Le Bacq, V. Beermann, S. Kühl, J. Herranz, S. Henning, L. Kühn, T. Assel, L. Guétaz, G. Renou, J. Drnec, P. Bordet, A. Pasturel, A. Eyckmüller, T. J. Schmidt, P. Strasser, L. Dubau, F. Maillard, *Nat. Mater.* **2018**, 17, 827; d) X. Li, X. Su, Y. Pei, J. Liu, X. Zheng, K. Tang, G. Guan, X. Hao, *J. Mater. Chem. A* **2019**, 7, 10745; e) X. Zhang, X. Sun, S.-X. Guo, A. M. Bond, J. Zhang, *Energy Environ. Sci.* **2019**, 12, 1334.
- [6] Z. Xia, S. Guo, *Chem. Soc. Rev.* **2019**, 48, 3265.
- [7] a) J. K. Nørskov, T. Bligaard, J. Rossmeisl, C. H. Christensen, *Nat. Chem.* **2009**, 1, 37; b) T. Zambelli, J. Winterlin, J. Trost, G. Ertl, *Science* **1996**, 273, 1688.
- [8] R. G. Mariano, M. Kang, O. J. Wahab, I. J. McPherson, J. A. Rabinowitz, P. R. Unwin, M. W. Kanan, *Nat. Mater.* **2021**, 20, 1000.
- [9] a) X. Fan, Y. Liu, S. Chen, J. Shi, J. Wang, A. Fan, W. Zan, S. Li, W. A. Goddard III, X. M. Zhang, *Nat. Commun.* **2018**, 9, 1809; b) S. Liu, Z. Hu, Y. Wu, J. Zhang, Y. Zhang, B. Cui, C. Liu, S. Hu, N. Zhao, X. Han, *Adv. Mater.* **2020**, 32, 2006034; c) R. G. Mariano, K. McKelvey, H. S. White, M. W. Kanan, *Science* **2017**, 358, 1187; d) Y. Sun, Y. Liang, M. Luo, F. Lv, Y. Qin, L. Wang, C. Xu, E. Fu, S. Guo, *Small* **2018**, 14, 1702259.
- [10] G. Kresse, J. Furthmüller, *Comput. Mater. Sci.* **1996**, 6, 15.
- [11] Y. Zheng, Y. Jiao, M. Jaroniec, S. Z. Qiao, *Angew. Chem., Int. Ed.* **2015**, 54, 52.
- [12] J. K. Nørskov, T. Bligaard, A. Logadottir, J. Kitchin, J. G. Chen, S. Pandelov, U. Stimming, *J. Electrochem. Soc.* **2005**, 152, J23.
- [13] A. Ruban, B. Hammer, P. Stoltze, H. L. Skriver, J. K. Nørskov, *J. Mol. Catal. A: Chem.* **1997**, 115, 421.
- [14] X. Gui, J. Wei, K. Wang, A. Cao, H. Zhu, Y. Jia, Q. Shu, D. Wu, *Adv. Mater.* **2010**, 22, 617.
- [15] V. Wang, N. Xu, J. C. Liu, G. Tang, W.-T. Geng, arXiv: 1908.08269, **2019**.
- [16] L. Yu, X. Pan, X. Cao, P. Hu, X. Bao, *J. Catal.* **2011**, 282, 183.